ESTIMATION OF FRIED'S PARAMETER FROM SPECKLEGRAMS OF SOLAR FEATURES

R. SRIDHARAN[1,*], P. VENKATAKRISHNAN[2] and V. K. VERMA[3]
[1]*Indian Institute of Astrophysics, Bangalore 560 034, India (e-mail: sridhar@prl.ernet.in)*
[2]*Udaipur Solar Observatory, Udaipur, Rajasthan 313 001, India (e-mail: pvk@prl.ernet.in)*
[3]*State Observatory, Manora Peak, Nainital 263 129, India (e-mail: verma@upso.ernet.in)*

(Received 10 August 2001; accepted 25 June 2002)

Abstract. A few methods of estimating Fried's parameter (r_0) from specklegrams of solar features are described. Some of these methods were used to estimate r_0 for the speckle data obtained from Kodaikanal Observatory (KO), Uttar Pradesh State Observatory (UPSO) and Udaipur Solar Observatory (USO). The average value of r_0 was found to be ~ 3 cm at USO and UPSO during our observations. At KO, values of r_0 ranging from 6 to 10 cm were estimated.

1. Introduction

The atmospheric turbulence is characterised by a spatial scale r_0, called Fried's parameter. There are many ways of interpreting this parameter: it is the size over which the r.m.s. phase fluctuations in the perturbed wave-front is 1 radian; a lens of diameter r_0 is capable of achieving a 30% Strehl definition and an angular resolution of the order of λ/r_0 (Fried, 1965); it is the coherence length of the complex amplitude of the perturbed wave-front (Ricort and Aime, 1979); it is the coherence diameter of the atmosphere (Goodman, 1985). It severely influences the quality of the images recorded using a ground-based telescope; the larger its value, the better is the quality. It is indeed a crucial parameter in evaluating good observing sites.

In general, the transfer function of an instantaneous image is an inseparable combination of the transfer function of the atmosphere and that of the telescope (Ricort and Aime, 1979). However, in the case of a long exposure image, the transfer function can be written as the product of the transfer function of the atmosphere and that of the telescope (Roddier, 1981). Hence, *if r_0 is known*, a long exposure image can be deconvolved, using the theoretical expression for the long exposure transfer function and linear filters like optimal and Wiener filtering (Press *et al.*, 1993; Gonzalez and Wintz, 1977) and the resulting image can be subjected to scientific study.

As the degradation produced by the atmosphere varies both with space (direction) and time, in stellar speckle interferometry the point spread function (PSF) is usually obtained by observing a point object in the direction close to the extended

*Presently at Udaipur Solar Observatory, Udaipur, Rajasthan, 313001 India.

Solar Physics **211:** 395–410, 2002.

object, immediately before or after recording its image. An ensemble average of the power spectrum of the PSF (known as speckle transfer function (STF)) is estimated from the recorded data and then used to compensate for the attenuation of the Fourier amplitudes of the object. Due to ubiquitous solar light, it is impractical to locate a point object in the sky during daytime observations. Consequently, in solar speckle interferometry, the Fourier amplitudes of the object are compensated using a theoretical transfer function, derived first by Korff (1973). *Again, knowledge of r_0 is essential to estimate the theoretical STF.*

In this paper, by studying a few methods of estimating r_0 from a series of short exposure images and their relative merits, we hope to identify a method that is best suited for solar speckle imaging. Several methods have been reported in the literature for estimating this parameter from solar images (Brandt, 1969, 1970; Aime *et al.*, 1978; Roddier, 1981; von der Lühe, 1984; Seykora, 1993). We briefly describe methods of estimation of r_0 in Section 2. In Section 3, we present the details of our speckle data recorded at Kodaikanal Observatory (KO), Kodaikanal, Uttar Pradesh State Observatory (UPSO), Nainital, and Udaipur Solar Observatory (USO), Udaipur, India. In Section 4 and 5 we describe the various preprocessing procedures and the methods for estimation of r_0 from speckle data recorded at KO, UPSO, and USO, respectively. In Section 6, we comment on the methods of estimating r_0. In the last section, we present the summary of the work carried out in this paper.

2. Methods of Estimating r_0

2.1. From angle-of-arrival fluctuations

Fried (1965) expanded the phase of the wave-front over a circular aperture (for example, at the entrance pupil of a telescope) in terms of a series of orthonormal polynomials, each representing a specific geometrical shape and found that the coefficient of the linear term is much larger than that of the spherical and quadratic terms for a given r_0 and diameter D of a telescope. He concluded that the random tilting of the wave-front is the major distortion. The random tilting of the wave-front from its average position causes fluctuations in the angle of arrival of the light rays (assumed to be normal to the surface of the wave-front). If β_x and β_y denote the fluctuations in the angle of arrival in x and y directions respectively, then the resultant fluctuation $\langle \beta^2 \rangle$ is given by (Fried, 1975)

$$\langle \beta^2 \rangle \equiv \langle \beta_x^2 \rangle + \langle \beta_y^2 \rangle = 0.357 \lambda^2 r_0^{-5/3} D^{-1/3}. \tag{1}$$

From Equation (1), it is clear that:

(1) For a given r_0 (i.e., for given seeing conditions), the mean square fluctuation in the angle of arrival of the light rays decreases as the diameter of the telescope increases.

(2) For a given D, the mean square fluctuation in the angle of arrival of the light rays decreases as r_0 increases; i.e., the image motion is small when the seeing is good.

The fluctuations in the angle of arrival of the light rays cause image motion at the focal plane of a telescope. The image of a point source obtained using small and medium sized telescopes moves randomly in the focal plane and the magnitude of the displacement depends on the seeing conditions. By carefully measuring the random displacement of the centroid of the image, the mean square fluctuation in the angle of arrival and r_0 can be estimated (Equation (1)).

2.1.1. *Error Estimation*

The error $\delta\beta$ in the measurement of β is approximately equal to the error $\delta\theta$ in the measurement of the displacement. The error δr_0 in the estimation of r_0 is given by $\delta r_0 = 1.2\, r_0\, \delta\theta/\beta$. Thus, δr_0 is directly proportional to the error or accuracy in the measurement of the displacement. In order to achieve higher accuracy in the measurement of the displacements, higher spatial sampling is necessary.

2.1.2. *Application to Images of Extended Sources*

When applied to images of extended sources, it is found that the high-frequency components of the image are more sensitive to the image motion than the low-frequency components. This is due to the fact that any given shift in the image is a larger fraction of the component with smaller period. The relative shift of an image with respect to a reference image can be estimated using a cross-correlation technique (von der Lühe, 1983) in terms of pixel/sub-pixel units and the variance can be estimated in arc sec. Smithson and Tarbell (1977) and von der Lühe (1983) have pointed out the need for subtracting a bi-linear fit of the form $B(x, y) = a_0 + a_1 x + a_2 y + a_3 xy$ from the data to avoid the shift in the peak of the auto-correlation function due to the presence of linear trends. This process will remove some of the low-frequency components. As the low-frequency components are less sensitive to the image motion than the high-frequency components, removing them does not alter the result. In other words, the correlation between the high-frequency components is sufficient for estimating the image shift.

2.1.3. *Limitations of the Method*

This method demands high spatial sampling. For example, to estimate r_0 with an accuracy of 10%, given $r_0 = 5$ cm, $\lambda = 6563$ Å, and $D = 30$ cm, image motion has to be measured with an accuracy of 0.1 arc sec. The accuracy is limited by the spatial sampling of the image. The accuracy can be improved by a factor of two using an interpolation algorithm (Niblack, 1986) for determining the peak of the cross-correlation function. This would imply that the sampling must be approximately 3 pixels per diffraction limit. For $D = 15$ cm with other parameters the same as given above and again assuming an accuracy of half-a-pixel, the spatial sampling needed would be nearly 5 pixels per diffraction limit. For small telescopes, this

would mean magnification of the image at least by a factor of 3. When filters with bandwidths of 0.5 to 1 Å are used, the light level would be decreased drastically.

The motion of the image at the focal plane is equivalent to the change in the tilt of the isophase surface of the wave-front at the aperture plane. The change in the tilt occurs within a duration of a few milliseconds (typically 10 ms). To measure the consecutive positions of the image exactly, the exposure time for each of the recorded image of a sequence should be less than or of the order of 10 ms. Thus, for faint stars, light level becomes a serious problem. Moreover, the seeing conditions do not remain constant for a long time and a large number of frames have to be recorded in a short ($\sim$ 1 min for solar observations (von der Lühe, 1993)) duration to achieve statistically significant results. Thus, *the need for short exposure times to freeze the atmosphere and the the need for high frame rate are some of the constraints on this method.*

It has been mentioned in the literature that one of the major drawbacks of this method is that the image motion due to the atmosphere cannot be distinguished from that due to improper tracking and vibrations of the telescope. In other words, this method is highly susceptible to tracking errors and can lead to incorrect estimation of the image motion due to the atmosphere. An alternate scheme that is insensitive to the tracking errors, popularly known as DIMM, has been developed by Fried (1975) and others (Sarazin and Roddier, 1990). It consists of two small apertures mounted on a single tracking system, separated by some distance. r_0 is estimated from the mean-square value of the difference in the angle-of-arrival fluctuations.

2.2. POWER-SPECTRUM EQUALISATION METHOD

In this method (Castleman, 1979; Stockham, Cannon, and Ingebretsen, 1975; Huang, Schreiber, and Tretiak, 1971; Andrews and Hunt, 1977), first the degraded image is segmented into square regions that are large compared to the extent of the degrading point spread function. For each segment, the power spectrum is estimated and the logarithm of power spectra are added together and an average power spectrum is obtained. If the scene under consideration is complex enough, the signal components tend to average out in the log power spectrum. The degrading transfer function does not get averaged out as it is constant throughout the region (as long as the region is smaller than an isoplanatic patch). In the absence of noise, the average power spectrum, approximately converges to the logarithm of the squared magnitude of the degrading transfer function. An important assumption in this method is that the object and the noise power spectrum are stationary. Though the atmospheric turbulence is not strictly stationary, it is believed to be locally homogeneous and isotropic and hence this method can be applied to long-exposure images.

2.2.1. *Implementation of the Method*

We implemented the following procedure to obtain the full width at half maximum (FWHM) of the degrading PSF from a single long exposure image.

Step 1: Divide the image into a number of segments, each of half the size of the original segment.

Step 2: Multiply the segments by a 100% Hanning window. This is basically to reduce the 'leakage error' (Bracewell, 1986).

Step 3: Estimate the power spectrum of these segments.

Step 4: Estimate the noise as the standard deviation of the power spectrum values of those pixels that are beyond the diffraction limit.

Step 5: Subtract the estimated noise from the power spectrum. Replace any small negative values of the order of 10^{-5} by zeros.

Step 6: Find the average log power spectrum of all the segments.

Step 7: Exponentiate the average power spectrum, find the square root and divide it by the telescope's transfer function.

Step 8: Find the inverse Fourier transform of the resulting function to obtain the PSF.

Step 9: Fit 1-D Gaussian to the cross-sections of the PSF (along x and y directions) and estimate the FWHM. The average value of the FWHM is converted into radians and then r_0 is estimated as λ/FWHM.

2.2.2. *Error Estimation*

If $\delta\theta$ is the error in the estimation of the FWHM corresponding to an error of δr_0 in r_0, then the error δr_0 in the estimation of r_0 is $\delta r_0 = r_0^2\,\delta\theta/\lambda = r_0\,\delta\theta/(\lambda/r_0)$. $\delta\theta$ is decided by the spatial sampling in the image. Again, we find that high spatial sampling reduces the error involved in the determination or r_0. However, for a given spatial sampling, error will be less for bad seeing conditions. In other words, the larger the r_0, the larger will be the error, for a given spatial sampling.

2.3. SPECTRAL RATIO METHOD

In this method (von der Lühe, 1984), the ratio ϵ of the squared modulus of the average Fourier transform of an image to the ensemble average of its modulus squared Fourier transform is used as a diagnostic of the seeing conditions at the time of observations. It is called 'spectral ratio' and is a function of the telescope and the seeing conditions alone. If the object under consideration contains structures beyond $\mathbf{q} = \alpha$, where $\mathbf{q} \equiv \mathbf{f}/(D/\lambda)$ is the normalised spatial frequency, $\mathbf{f}$

is the spatial frequency and $\alpha \equiv r_0/D$ is the modified Fried's parameter, then ϵ steeply decreases beyond this limit. When the ensemble average of ϵ is expressed as a function of α and $\mathbf{q}$, isocontour lines satisfy the relation

$$\alpha = Aq^B, \quad \forall\ \alpha \leq 0.3, \tag{2}$$

where A and B are constants. While applying this method to real data, first the theoretical value of the spectral ratio is estimated and constants A and B are determined for various values of ϵ. A log–log plot of $E(\epsilon(\mathbf{q}))$ vs. $\mathbf{q}$ is then obtained for the observed data and the ratio obtained from theoretical models is overplotted. The normalised frequency $\mathbf{q}$ at which the slopes of the theoretical and observed spectral ratios match closely is determined and the corresponding spectral ratio is identified. Then the constants A and B corresponding to the identified spectral ratio are inserted in Equation (2) and α and r_0 are determined. The following two conditions should be met for the successful application of this method: (1) The total duration of observation should be short enough to justify ergodicity hypothesis. (2) The total number of images recorded should be large enough to ensure that the arithmetic average is equal to the ensemble average.

2.3.1. *Error Estimation*

If δA, δB, and $\delta\mathbf{q}$ are the errors in the measurement of A, B and $\mathbf{q}$ respectively, then the most probable error δr_0 (Bevington and Robinson, 1992) in the measurement of r_0 is $\delta r_0 = r_0[(\delta A/A)^2 + (\delta\mathbf{q}/\mathbf{q})^2 + (\delta B \log \mathbf{q})^2]^{1/2}$. Thus, the accuracy of the result depends on the accuracy of the measurements of $A(\epsilon)$ and $B(\epsilon)$, $\mathbf{q}$ and $|\mathbf{q}|$. $\delta\mathbf{q}$ can be assumed to be equal to the smallest spacing in the Fourier domain expressed in normalised spatial frequency units. If we assume that A and B are measured with high accuracy such that $\delta A = 0$ and $\delta B = 0$, then the percentage error in r_0 is proportional to the percentage error in $\mathbf{q}$. As $|\mathbf{q}|$ is limited to the range 0.2 to 0.3 (von der Lühe, 1984), the accuracy of the estimation increases when $|\delta\mathbf{q}|$ is small. In other words, better accuracy can be obtained when this method is used for a large telescope ($D \gg r_0$). Even when δB is non-zero, the error in r_0 is less when $|\mathbf{q}|$ is small as implied by the third term in $(\delta r_0)^2$. Unlike the methods described earlier, this method does not demand very high spatial sampling.

3. Observational Data

To estimate the Fried's parameter from specklegrams of solar features we have used observational data recorded at KO, UPSO, and USO. A brief introduction of their telescopes, instruments and recorded solar images is found in Sections 3.1, 3.2, and 3.3, respectively.

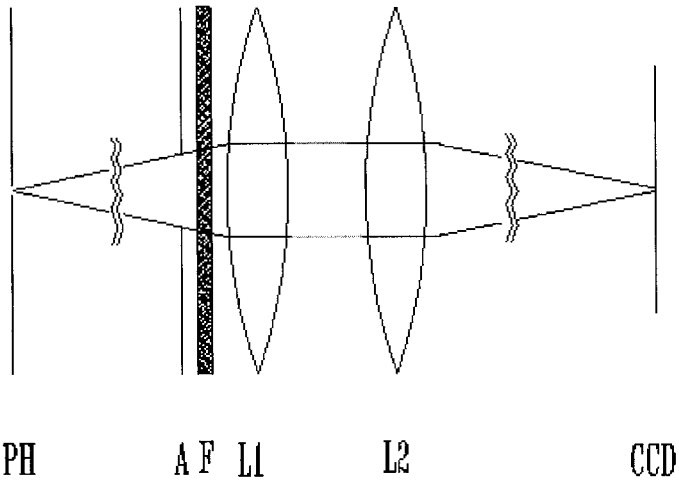

Figure 1. The re-imaging unit consists of: pinhole PH, which selects a portion of the Sun's image; aperture A of 5 mm diameter; Hα filter F; collimating lens $L1$; camera lens $L2$; charge coupled device (CCD).

3.1. KODAIKANAL OBSERVATORY DATA

Speckle imaging observations were performed on 2, 3, and 4 August 1998 between 1:00 and 5:30 UT, with the 38-cm tunnel telescope of the Kodaikanal Observatory (KO) (Bappu, 1967) using a re-imaging unit shown in Figure 1. The pupil plane was re-imaged using a 300 mm $f/5$ collimator. A 5-mm aperture and a filter with 160 Å bandpass, centered at 6520 Å, were placed in the diverging beam close to the collimator. The collimated beam was focused on to a EEV^{TM} camera P46582 consisting of 578 $\times$ 576 pixels of size 15 $\times$ 22.5 micron. The images were acquired using a DT2861 frame grabber card which also re-sampled each row of the image into 512 pixels. Only the central 128 $\times$ 64 pixels were activated using the hardware windowing capability of the frame grabber card and used to record the image of a pinhole of 1.5 mm diameter. This resulted in a circular field of view of about 8.25 arc sec in size, with 0.0931 arc sec per pixel along a row and 0.12375 arc sec per pixel along a column. The theoretical resolution limit of the telescope is 0.43 arc sec at 6520 Å.

Several sets of images of a few sunspots and pores were recorded. Each set consisted of two sequences separated by about 17 s. Each subset consisted of sixteen frames (the maximum number of buffers available in the frame grabber card) with an exposure time of 1 ms per frame. The interval between the consecutive frames in a subset was about 88 ms. The observations were accompanied by regular dark-current and flat-field (defocused quiet regions) images.

3.2. Uttar Pradesh State Observatory data

Four sequences of images of an isolated sunspot and three sequences of images of a spot pair were recorded on on 2 June 1999 between 01:17 and 03:20 UT with the 15 cm Coude telescope of Uttar Pradesh State Observatory (UPSO) (Verma, 1999). The primary image was magnified using a Barlow lens. A Halle Hα filter with 0.5 Å bandwidth was placed near the focus. A 12 bit EEV37 camera consisting of 512 $\times$ 512 pixels of size 15 micron, cooled by a liquid circulatory unit, was used to record 1000 frames per sequence at the rate of $\sim$ 40 frames per s with an exposure time of 7 ms per frame. The recorded field of view was 65 $\times$ 65 arc sec in size with 0.65 arc sec per pixel. Five dark current and 100 flat-field (twilight sky) frames were recorded. The theoretical resolution limit of the telescope is 1.1 arc sec at 6563 Å.

3.3. Udaipur Solar Observatory Data

Sixteen sequences of images of a sub-flare region and twenty eight sequences of images of another sub-flare region, both belonging to the NOAA AR8898 were recorded on 9 March 2000 between 05:30 and 07:00 UT with the 13.5-cm Coudé telescope of Udaipur Solar Observatory (USO) (Ambasta, 1999). The selected region of the primary image was re-imaged using a combination of two lenses. A Halle Hα filter with 1 Å bandwidth was placed between the two lenses. The 8-bit photometric CCD camera consisting of 768 $\times$ 493 pixels of size 11 $\times$ 13 micron was used to record 100 frames per sequence at the rate of 1.2 frames per s with an exposure time of 20 ms per frame. The recorded field of view was 57.6 $\times$ 67.8 arc sec with 0.45 arc sec per pixel along a row and 0.53 arc sec per pixel along a column. The theoretical resolution limit of the telescope is 1.22 arc sec at 6563 Å.

4. Pre-Processing

4.1. Dark and flat-field corrections

Average dark and flat-field images are obtained from the recorded series of dark and flat-field images. The images of the object are corrected using the standard procedure (McLean, 1989). When the flat-field images contain artifacts due to dust specks, the procedure described by von der Lühe (1993) is adopted to minimise their effect. However, it should be noted that Equation (4) of that paper is erroneous and should be modified to

$$\bar{f}(x) = \frac{a(x)}{\bar{a}(x)}[f(x) - d(x)] + d(x), \tag{3}$$

where the symbols have the same meaning as mentioned in that paper.

4.2. REGISTRATION

In general, a sequence of images obtained from a ground-based telescope will have motion due to atmosphere as well as imperfect tracking. The image motion due to the telescope is coherent over the entire field of view. The images of the sequence can be aligned using cross-correlation technique (von der Lühe, 1983). When used to align the images that contain a large number of isoplanatic patches, this technique would detect only the coherent motion of the entire field of view. This fact is used to align the images to account for tracking errors alone. To detect the image motion due to atmosphere, the images have to be segmented into several isoplanatic patches and a bi-linear least square surface has to be subtracted from each of segments. The cross-correlation gives the amount of shift needed to align a given image with a reference image with pixel accuracy. However, the accuracy can be improved by a factor of two using an interpolation method (Niblack, 1986). The necessary shifts are incorporated by multiplying the Fourier transform of the image by a phase factor $\exp(2\pi\, \jmath\, (k_x x/m + k_y y/n))$, where m and n are the number of pixels along a row and column of the image respectively and x and y are the required shifts in the corresponding directions.

4.3. DE-STRETCHING

When the field of view of the recorded image is much larger than the size of the isoplanatic patch, different portions of the image move differently and hence the image gets distorted. The process of removing the effects of anisoplanatic image motions from a time series of images is called *de-stretching* (November, 1986; Topka, Tarbell, and Title, 1986). For de-stretching our images, we used a portion of the software package developed by the scientific staff of Sacramento Peak observatory. The package was provided by Keil (2000) of the observatory. Essentially, we used this package to get a registered image sequence. In what follows, we refer to this truncated processing as 'destretching'.

4.4. FRAME SELECTION

Most often it is convenient to select the best images from a series of images for further analysis (reference image in de-stretching, for example). A few bad images of a series of images recorded during moderate seeing conditions can significantly alter the gain obtained from a few best images. We characterised each image by its contrast (or sharpness) and identified the image having the highest contrast as the best image of the series. The contrast is estimated as the ratio of the sum of mean square intensity gradient in x and y directions and the mean intensity squared (Scharmer, 2000),

$$C = \sum_{m,n} ((I(m+d,n) - I(m,n))^2 + (I(m,n+d) - I(m,n))^2)/(\bar{I})^2, \qquad (4)$$

where d can be selected as the number of pixels within the diffraction limit or a pixel more than that.

4.5. FRAME SEGMENTATION

The step after pre-processing and de-stretching a sequence of images is to divide each image into several overlapping segments that are smaller than the typical size of the isoplanatic patch. We followed the procedure described by von der Lühe (1993). We repeat the segmentation process for all the images of a sequence and form a 'sub-image sequence' with the corresponding segments of the sequence. We estimate r_0 for each sub-image sequence.

5. Estimation of r_0

5.1. KO DATA

As mentioned earlier, the frame grabber re-sampled the image along a row. Moreover, the video input supplied by the camera was ac-coupled and dc-restored. Thus, there was no one-to-one correspondence between the pixels in the CCD and the digitised images. Because of these reasons, we could not do meaningful flat-field corrections. However, while analysing the speckle data, we selected only those small scale features that were away from the location of dust specks in the flat-field images. We used the frame to frame motion of the features as an indicator of their solar origin. We selected rectangular windows, centered at the feature of interest from the recorded images and re-sampled them to have identical plate scale along the rows and columns. We 'de-stretched' the images when the selected field of view exceeded 4 arc sec. We estimated r_0 using spectral ratio method for a few data sets. For two sub-sets (consisting of 16 images) of a pore region, (comprising 4 overlapping segments, each of ~ 3 arc sec) the average value was found to be 9 ± 3 cm. For two sub-sets (consisting of 16 images) of a sunspot region, (comprising 4 overlapping segments, each of ~ 3 arc sec) the average value was found to be 7 ± 3 cm. The huge error bars could be due to estimating r_0 from just 16 frames. Moreover, in the absence of flat-field images, noise could not be estimated reliably.

5.2. UPSO DATA

The images of the three sequences of a sunspot and four sequences of a spot pair were pre-processed using the procedure described in the previous section. The registered, rescaled images had 128 pixels in either directions with a field-of-view of 62.4 arc sec square. We estimated r_0 by all the three methods described in Section 2. As the power spectrum equalisation method failed to produce any meaningful results, we present the results obtained from the other two methods in this section.

TABLE I

Comparison of r_0 estimated from two different methods.

Seq.	ARF (cm)	SR (cm)	C	RC	Remarks
1	3.98±0.73	3.11±0.88	0.37	0.54	single sunspot
2	3.93±0.74	2.98±0.79	0.34	0.36	single sunspot
3	4.11±0.80	3.05±0.83	0.34	0.43	single sunspot
4	3.55±0.62	3.11±0.88	0.32	0.44	single sunspot
5	3.21±0.51	2.83±0.71	0.53	0.63	spot pair
6	3.42±0.58	2.86±0.71	0.53	0.61	spot pair
7	3.60±0.64	2.87±0.71	0.48	0.52	spot pair

Note: ARF – from angle-of-arrival fluctuations; SR–spectral ratio method. C is the correlation coefficient of average contrast of the segments and the corresponding r_0 estimated from spectral ratio method and RC is the corresponding Spearman's rank correlation coefficient. The significance of rank correlation (probability of the hypothesis that the data are uncorrelated) was less than 10^{-8}.

5.2.1. *Estimation of r_0 from Angle-of-Arrival Fluctuations*

The registered images were divided into a number of overlapping segments of size 32×32 pixels (15.6 arc sec square) as explained earlier and r_0 was estimated for each segment, using all the corresponding segments of the sequence of (~ 920) images as explained in Section 2.1. The analysis was restricted only to the centre of the field of view and the segments that were near the edges of sunspots were neglected. The procedure was repeated for all the seven sequences and the average value of r_0 for the sequences was found to be 3.7 ± 0.7 cm.

5.2.2. *Spectral Ratio Method*

We estimated r_0 using the spectral ratio method for all the registered, 'de-stretched' image sequences. We restricted the analysis to only segments of size 16×16 pixels (7.8 arc sec square). For each sequence, the images were divided into 225 overlapping segments and r_0 was estimated for all the segments. For all the sequences, the average value of r_0 was found to be 3.26 ± 0.57 cm.

Table I shows average values of r_0 estimated using the two methods for all the sequences.

5.3. USO DATA

All the 28 sequences of images of a sub-flare region were subjected to dark and flat-field corrections and then registered using the procedure described earlier. The size of images in the registered sequences varied from one sequence to the other, with a typical size of 36×63.6 arc sec. A comparison of this size with the ini-

tial size 57.6 × 67.8 arc sec of the recorded images implies significant tracking errors. For each sequence, a square window of size 36 arc sec was selected from the registered images and then re-sampled to have 128 pixels in either direction. As the tracking of the telescope was poor, it was meaningless to estimate Fried's parameter from the angle-of-arrival fluctuations. The power spectrum equalisation method produced unrealistic values of r_0.

We estimated r_0 using spectral ratio method. First, we estimated the theoretical spectral ratios using the speckle transfer functions and short exposure transfer functions for various values of D/r_0, with r_0 ranging from 2 to 10 cm in steps of 0.1 cm for an array size of 32 × 32 pixels. We estimated the constants A and B (Equation (2)) for various values of spectral ratios ranging between 0.2–0.9 in steps of 0.001. Then we divided the images into segments of size 32 × 32 pixels (9 arc sec) and estimated the spectral ratios for each of the segments. By comparing the slopes of the observed spectral ratios with the theoretical ratios in a log–log plot of spectral ratio ϵ vs. normalised spatial frequency $\mathbf{q}$ in the frequency range of 0.1–0.4, we estimated the spectral ratio. Then using the corresponding constants A and B, we inferred r_0. We also estimated the error as described in Section 2. We repeated the procedure for all the 28 sequences of images.

5.3.1. *Spatial and Temporal Variation of* r_0

Figure 2 shows the spatial distribution of r_0 estimated for all the 28 sequences. For each sequence, we obtained the average value r_0 over the field of view (average of r_0 values of all the 49 segments). Figure 3 shows the variation of r_0 with time. The time-interval between consecutive sequences was not uniform but varied between 30 s to 1 min. The duration of acquisition of a sequence was ∼ 82 s. Consequently, the time interval is not uniform in the plot. An approximate value of 112 s (82 + 30 s) has been assumed as an interval between the consecutive estimates. It indicates the variation of r_0 over an hour duration. Table II gives the average (spatial average) value of r_0 for each of the sequences. The linear and Spearman's rank correlation coefficient of the estimated r_0 values with the average contrast of the segments are also tabulated. The probability that two given populations are uncorrelated with each other is given by the 'significance' of the rank correlation coefficient; that is, higher the correlation between the populations, smaller the significance of the rank correlation coefficient. We find that in most of the cases, the correlation is significant (very low significance of the rank correlation coefficient) indicating the fact that higher contrast values correspond to higher r_0. There are a few sequences where the significance of the rank correlation is more than 0.1.

We estimated r_0 corresponding to 16 sequences of another sub-flare region in a similar manner. The average value was found to be 3.5 ± 0.8 cm.

TABLE II

r_0 estimated from USO data by spectral ratio method.

Seq.	r_0 (cm)	C	RC	S	Seq.	r_0 (cm)	C	RC	S
1	3.37±0.59	0.42	0.38	7×10^{-3}	15	3.35±0.56	0.45	0.46	8×10^{-4}
2	3.47±0.60	0.22	0.21	1×10^{-1}	16	3.04±0.49	0.66	0.77	1×10^{-11}
3	3.52±0.60	0.29	0.32	2×10^{-2}	17	3.10±0.52	0.55	0.59	6×10^{-6}
4	3.42±0.58	0.49	0.52	1×10^{-4}	18	3.11±0.55	0.63	0.69	3×10^{-8}
5	3.03±0.51	0.47	0.68	5×10^{-8}	19	3.02±0.53	0.68	0.73	1×10^{-9}
6	3.20±0.56	0.56	0.72	6×10^{-9}	20	3.24±0.54	0.42	0.43	1×10^{-3}
7	3.18±0.53	0.68	0.71	1×10^{-8}	21	3.08±0.54	0.50	0.47	5×10^{-4}
8	3.41±0.57	0.45	0.45	1×10^{-3}	22	3.32±0.55	−0.10	−0.02	9×10^{-1}
9	3.34±0.57	0.66	0.68	5×10^{-8}	23	3.22±0.56	0.47	0.54	5×10^{-5}
10	3.25±0.56	0.31	0.55	4×10^{-4}	24	3.46±0.61	0.09	0.01	9×10^{-1}
11	3.52±0.58	0.27	0.18	2×10^{-1}	25	3.42±0.57	0.30	0.29	4×10^{-2}
12	3.29±0.57	0.31	0.42	2×10^{-3}	26	3.10±0.53	0.67	0.63	1×10^{-6}
13	3.17±0.54	0.58	0.57	1×10^{-5}	27	3.42±0.56	0.30	0.29	3×10^{-2}
14	2.83±0.53	0.56	0.63	2×10^{-5}	28	3.39±0.60	0.47	0.44	1×10^{-3}

Note: linear and Spearman's rank correlation coefficients (C and RC, respectively) of the estimated r_0 with the average contrast of the segments for all the sequences are given. S denotes the significance of the rank correlation.

6. Comments on Various Methods of Estimating r_0

The method of estimation of r_0 from angle-of-arrival fluctuations demands high spatial and temporal sampling. Image motion caused by improper tracking is coherent over the entire field of view and can be estimated using cross-correlation technique. However, the results are not accurate for the regions near the edges of the field of view. Moreover, this method is sensitive to the scene (sunspots, for example) under consideration. Power spectrum equalisation method might work in situations where the assumption of stationarity is valid and the size of the image is much larger than the degrading PSF. But it demands high spatial sampling. As this method failed to produce any meaningful results, we do not recommend this method for solar observations. Spectral ratio method seems to be the most widely applicable method and is well suited for speckle observations, as r_0 is estimated from the data itself. It does not require very high spatial sampling; it is independent of the scene under consideration. However, this involves visual comparison of the observed profiles of the spectral ratio ($\epsilon(\mathbf{q})$) with those obtained from theoretical model. While the theoretical STF (Korff, 1973) itself has associated uncertainty due to finite bandwidth, its numerical evaluation is highly time consuming for large array sizes. Aime *et al.* (1978) have prescribed a method to estimate r_0 from a series of observations based on the distinct behavior of the (STF) at low and high

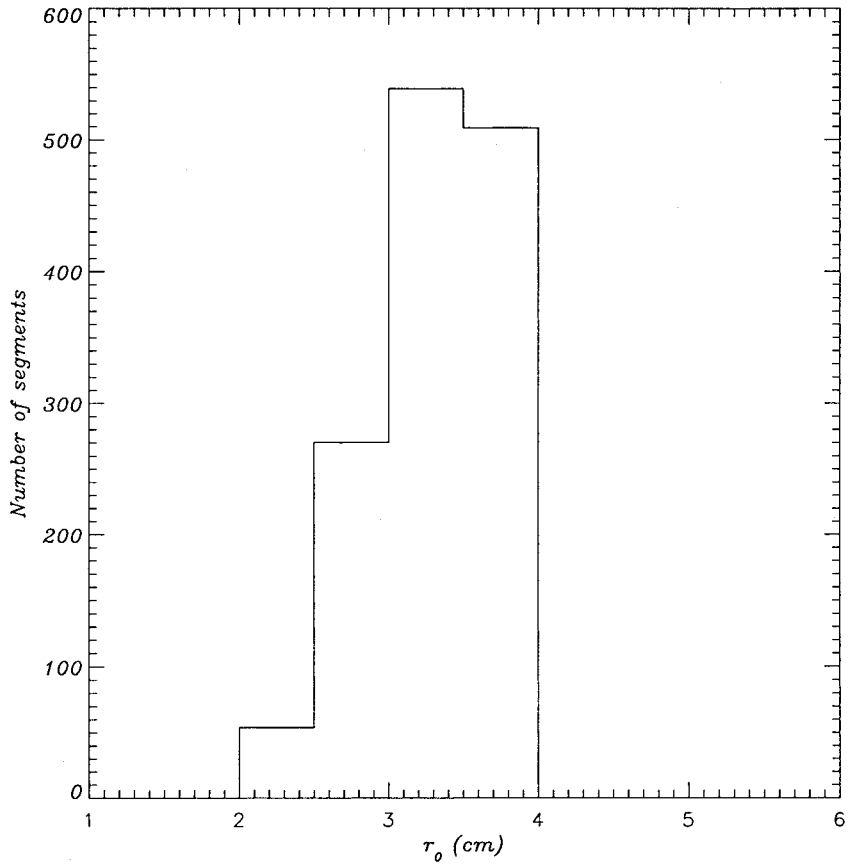

Figure 2. Spatial distribution of r_0 estimated using spectral ratio method for 28 sequences a sub-flare region. In each sequence, the images were divided into 49 segments each of size 32 pixels square (9 arc sec). The total number of segments is 1372. The bin-size is 0.5 cm.

spatial frequencies. The method seems to fail when the differences of the r_0 values of two independent observations are small or the lifetime of small-scale features is smaller than time interval between two independent observations. Seykora (1993) has proposed a method of estimating r_0 from scintillation measurements. This method can be applied only to extended objects; that is, over a large field of view. It is suitable for measuring the atmospheric seeing at different heights. Krishnakumar and Venkatakrishnan (1997; also Krishnakumar, 1998) have proposed a method to estimate r_0 through a parametric search method. This method works well for stellar images, but needs modification before it can be applied to solar images.

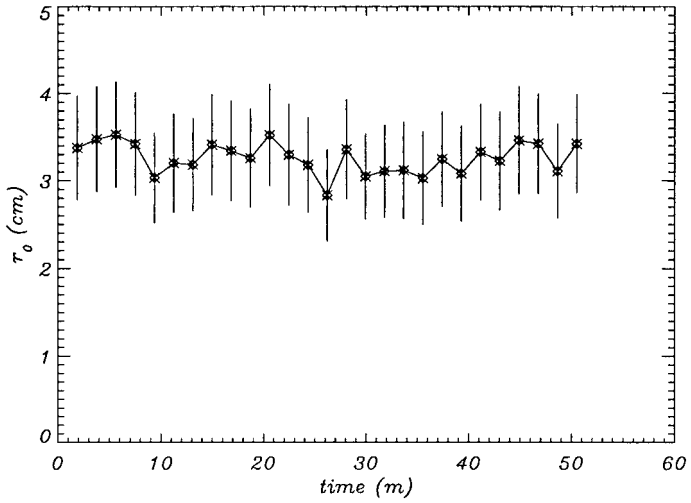

Figure 3. Variation of r_0 with time (USO data). Variation of average (spatial) r_0 with time. As the time interval between the sequences was not uniform, an approximate value of 112 s has been assumed to be the interval between the sequences.

7. Summary

In this paper, we have described the details of speckle imaging observations performed at KO, UPSO, and USO. We have described the methods of pre-processing that we adopted for analysing the speckle data. We have explored the possibility of estimating r_0 from three different methods. We have used some of these methods to estimate r_0 for our speckle data. We found that in all these methods, the estimated value of r_0 has an error of 25%. While estimating r_0 from the fluctuations in the angle of arrival of the light, we found that high-frequency components are more sensitive to the image motion than the low-frequency components. The spectral ratio method seems to be the most suitable method for speckle data. The average value of r_0 at USO and UPSO was $\sim 3 \pm 0.7$ cm on days when these observations were performed. These were the values of r_0 at the time of observations on those days and should not be considered as average values of r_0 on these places. At KO, the values of r_0 ranging from 6–10 cm were observed on the three days of observations described earlier in this paper.

Acknowledgements

We thank Prof. Steve Keil for providing the 'destretching' code. One of the authors (R. Sridharan) thanks Mr B. L. Paneri and Mr Dal Chand of USO and Mr P. Devendran and M. H. Hariharan of KO for their help during the observations. We also thank the referee for his useful and enlightening comments on the initial version of this paper.

References

Aime, C., Ricort, G., Roddier, C., and Lago, G.: 1978, *J. Opt. Soc. Am.* **68**, 1063.

Ambasta, A.: 1999, *Space Research in India: Accomplishments and Prospects-Solar Optical Astronomy at Udaipur Solar Observatory*, PRL Alumni Association, Ahmedabad.

Andrews, H. C. and Hunt, B. R.: 1977, *Digital Image Restoration*, Prentice-Hall, Inc., Englewood Cliffs, New Jersey.

Bappu, M. K. V.: 1967, *Solar Phys.* **1**, 151.

Bevington, P. R. and Robinson, D. K.: 1992, McGraw-Hill, Inc., New Delhi.

Bracewell, R. M.: 1986, *Fourier Transform and Its Applications*, second, revised edition. McGraw-Hill International Editions, New Delhi.

Brandt, P. N.: 1969, *Solar Phys.* **7**, 187.

Brandt, P. N.: 1970, *Solar Phys.* **13**, 243.

Castleman, K. R.: 1979, *Digital Image Processing.* Prentice-Hall, Inc., Englewood cliffs, New Jersey.

Fried, D. L.: 1965, *J. Opt. Soc. Am.* **55**, 1427.

Fried, D. L.: 1975, *Radio Sci.* **10**, 71.

Gonzalez, R. C. and P. Wintz: 1977, *Digital Image Processing*, Addison-Wesley Publishing Company, London.

Goodman, J. W.: 1985, *Statistical Optics*, John Wiley and Sons, New York.

Huang, T. S., Schreiber, W. F. and Tretiak, O. J.: 1971, *Image Processing*, Vol. 59, p. 1586.

Keil, S.: 2000, Private communication.

Korff, D.: 1973, *J. Opt. Soc. Am.* **63**, 971.

Krishnakumar, V.: 1998, 'High-Resolution Imaging of Sun'. Ph.D. thesis, Indian Institute of Astrophysics and Bangalore University, Bangalore.

Krishnakumar, V. and Venkatakrishnan, P. V.: 1997, *Astron. Astrophys. Suppl. Ser.* **126**, 177.

McLean, I. S.: 1989, *Electronic and Computer-Aided Astronomy: From Eyes to Electronic Sensors*, ch. 8, Ellis Horwood Ltd. and John Wiley and Sons, New York.

Niblack, W.: 1986, *An Introduction to Digital Image Processing*. Prentice Hall International, New Jersey.

November, L. J.: 1986, *Appl. Opt.* **25**, 392.

Press, H. W., Teukolsky, S. A., Vellerling, W. T., and Flannery, B. P.: 1993, *Numerical Recipes in FORTRAN; the Art of Scientific Computing*, 2nd ed., Cambridge University Press, New Delhi.

Ricort, G. and Aime, C.: 1979, *Astron. Astrophys.* **76**, 324.

Roddier, F.: 1981, *Progr. Optics* **XIX**, 281.

Sarazin, M. and Roddier, F.: 1990, *Astron. Astrophys.* **227**, 294.

Scharmer, G. B.: 2000, Private communication.

Seykora, E. J.: 1993, *Solar Phys.* **145**, 389.

Smithson, R. and Tarbell, T. D.: 1977, *Correlation Tracking Study for Meter-Class Solar Telescope on Space Shuttle*, Palo Alto Research Lab., Palo Alto.

Stockham, T. G., Cannon, T. M., and Ingebretsen, R. B.: 1975, *Proc. of the IEEE*, Vol. 63. p. 678.

Topka, K. P., Tarbell, T. D., and Title, A. M.: 1986, *Astrophys. J.* **306**, 304.

Verma, V. K.: 1999, in T. R. Rimmele, K. S. Balasubramaniam, and R. R. Radick (eds.), *High Resolution Solar Physics,: Theory, Observations, and Techniques*, Vol. 183. p. 288.

von der Lühe, O.: 1983, *Astron. Astrophys.* **119**, 85.

von der Lühe, O.: 1984, *J. Opt. Soc. Am. A* **1**, 510.

von der Lühe, O.: 1993, *Astron. Astrophys.* **268**, 374.